P H Y S I C A L R E V I E W L E T T E R S

Pattern Formation in Self-Propelled Particles with Density-Dependent Motility

F. D. C. Farrell,[1] M. C. Marchetti,[2] D. Marenduzzo,[1] and J. Tailleur[3]

[1]*SUPA, School of Physics and Astronomy, University of Edinburgh, Mayfield Road, Edinburgh EH9 3JZ, United Kingdom*
[2]*Physics Department and Syracuse Biomaterials Institute, Syracuse University, Syracuse, New York 13244, USA*
[3]*Laboratoire Matiere et Systemes Complexes, Universit Paris Diderot, 75205 Paris, France*

We study the behavior of interacting self-propelled particles, whose self-propulsion speed decreases with their local density. By combining direct simulations of the microscopic model with an analysis of the hydrodynamic equations obtained by explicitly coarse graining the model, we show that interactions lead generically to the formation of a host of patterns, including moving clumps, active lanes, and asters. This general mechanism could explain many of the patterns seen in recent experiments and simulations.

Collections of self-propelled (SP) particles provide the most common realization of active matter, the study of which constitutes a rapidly growing area of research [1]. Examples of SP particles are bacteria, cells [2], and actin filaments "walking" on a carpet of immobilized molecular motors [3].

The term "active" is used to contrast these systems with their passive counterparts, such as solutions of diffusing Brownian particles. Active systems exhibit a much richer physics, in particular having a far greater tendency to form patterns. For instance, bacterial colonies of *E. coli* or *S. typhimurium* growing in the lab can self-organize into crystalline or amorphous arrangements of high-density bacterial clumps [4], while biofilms form even more elaborate patterns such as microbial honeycombs, essentially hexagonal lattices of low-density voids [5]. Similarly, actin in high density motility assays [3] organize in moving spots, stripes, and traveling waves.

What is the mechanism underlying the formation of these "active patterns?" One may expect that, as the underlying constituents of each system are so different, the answer to this question should also be system-specific. If we are to capture all details of a given active pattern, this is indeed likely to be the case. Yet, a fascinating possibility is that there may exist some generic origin of many of these patterns, stemming from a few universal key features of activity, linked to its inherent nonequilibrium nature. In some cases, pursuing such minimal descriptions can be very rewarding. A well-known example is the hydrodynamic theory of flocking proposed by Toner and Tu in [6], which was inspired by the "agent-based" model of Vicsek *et al.* [7]. The latter studied the dynamics of an ensemble of SP particles subjected to aligning interactions, whose ultimate origin may be hydrodynamic or collision-dominated in the cases of bacteria and actin filaments, or more complex for bird flocks or fish schools. Universal features successfully predicted by generic flocking models are spontaneous motion [6–8], giant density fluctuations [9,10], and the emergence of complex spatiotemporal active patterns [10,11].

The original Vicsek model considers point particles of fixed speed and includes no interactions between them other than a rule that aligns their velocities. Recently, focus has shifted onto specific models where additional interactions are included, most commonly steric repulsion [12–18]. Our aim here is to develop a more generic model for interacting SP particles. Interactions are incorporated in our model by assuming that the motility of the SP particles is a decreasing function of their local density [19]. One may envisage several physical mechanisms responsible for a decay of the propulsion velocity with density: here we highlight just two. First, such a slowing down may arise due to local crowding and steric hindrance, just as in [13,14,16,17]. An alternative mechanism can be provided by biochemical signaling such as quorum sensing in bacterial colonies, as recently explored theoretically [20] and experimentally [21]. This second mechanism may lead to slowdown even in dilute suspensions. Our work describes the results of simulations of a microscopic SP particles model with both interactions and alignment rule, the derivation of the corresponding hydrodynamic description of the model in terms of a density and a polarization field, and an analysis of the continuum theory. It therefore provides a direct bridge between microscopic and continuum models, which allows us to identify universal mechanisms driving pattern formation in interacting SP particles. As we shall see, interactions lead to an even larger repertoire of patterns in active particle suspensions than obtained in conventional Vicsek models. These include moving clumps, lanes, and asters (i.e., inward pointing defects of the polarization field with topological charge $+1$), and qualitatively match the patterns found experimentally, e.g., in [3].

We consider a modified version of the Vicsek model [7], where N particles in a box of size L^2 (hence, with overall mean density $\rho_0 = N/L^2$) interact via a pairwise aligning forcing, which simplifies the coarse graining of the microscopic model. In 2D the position r_i and direction, identified by an angle θ_i (or a vector $\mathbf{e}_{\theta_i}$), of the ith particle evolve according to

$$\dot{r}_i = v\mathbf{e}_{\theta_i}; \dot{\theta}_i = \gamma \sum_{j=1}^{N} F(\theta_j - \theta_i, r_j - r_i) + \sqrt{2\epsilon}\,\tilde{\eta}_i(t), \quad (1)$$

where γ and ϵ describe strength of alignment and fluctuations respectively, and $\tilde{\eta}(t)$ is a Gaussian white noise with zero mean and unit variance. F controls the alignment interactions between the spins. For simplicity, we choose $F(\theta, r) = \sin(\theta)/\pi R^2$ if $|r| < R$ (hereafter we restrict to $R = 1$) and 0 otherwise. This simple choice for F enforces polar alignment of the SP particles and will allow us to make progress anaytically, but we expect our results to extend to far more general forms of polar alignment. In the $v \to 0$ limit, our model is an off-lattice analogue of the XY model for a ferromagnet; hence, we call it the flying XY model. Last, a density-dependent velocity is introduced in the model by stipulating that v depends on the number of particles n within a given radius R_n, as $v(n) = v_0 e^{-\lambda n} + v_1$, where $v_0 \gg v_1 > 0$ are the dilute and crowded limiting velocities respectively, and $\lambda > 0$ controls the decay of the motility decreases with increasing density. Hereafter, we restrict to $R_n = R$.

Figure 1(a) shows a representative phase diagram of the flying XY model in the (ϵ, λ) plane for $N = 3000$ [22]. For small λ, when v is quasiconstant, the phases observed are the same as those in the literature on flocking models [7,10]. Namely, at high ϵ we find a disordered, homogeneous state [region c in Fig. 1(a)], followed by a polarly ordered phase with high density stripes [named stripy phase, b, in Fig. 1(a)] below a critical noise value. For even lower ϵ, we observe a "fluctuating flocking state" (region a) with polar order and large density fluctuations—this state is close to the one described in Refs. [10,11], and we do not discuss it further here. All these phases are expected by analogy with the Vicsek model.

Above a critical value $\lambda_c(\epsilon)$, new patterns appear. Due to the density-dependent motility, the SP particles cluster via
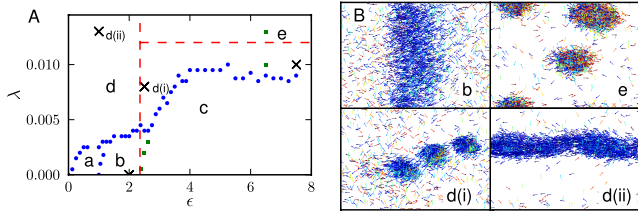
a self-trapping mechanism through which they assemble and slow down, creating a positive feedback loop akin to the one in [20]. This process leads to the formation of high-density clumps which slowly coarsen towards a fully phase-separated steady state. The Vicsek-like alignment tendency greatly affects this instability. On one hand, the critical value $\lambda_c(\epsilon)$ decreases almost to zero with decreasing ϵ. Furthermore, the presence of polar order promoted by the alignment changes the nature of the clusters. In Fig. 1(a), we identify at least three distinct patterns, of which snapshots are shown in Fig. 1(b). When ϵ is small, rather than structureless dots, the clusters show an orientational order and move coherently: they form "moving clumps" [pattern d(i) in Fig. 1]. For low ϵ and large λ the moving clumps merge into bands, or lanes [labelled as d(ii)]—within these, however, particles move parallel rather than perpendicular to the band, in contrast with the $\lambda \to 0$ stripy phase. Although we cannot rule out that the lane and moving clump "phases" may merge in the thermodynamic limits, they appear as distinct up to the largest system we simulated, with $N = 48\,000$ [23] [and ρ as in Fig. 1(a)]. Lanes are somewhat reminiscent of the "streaks" of actin filaments observed in [3]—it would be interesting to compare the dynamics of pattern formation in experiments and simulations to probe how similar the two really are. Finally, in the disordered, high ϵ phase, the clusters instead diffuse randomly and are, on average, stationary. Here, a temporal average of the particle orientation patterns shows that the clusters are asters (the aster phase is labeled as e in Fig. 1). However, as discussed in greater detail below, the orientation in the aster is nonstandard: particles point towards its center at the core, but they coherently point outwards in its periphery. We stress that moving clusters, lanes, and asters are not observed either in the standard Vicsek model [7,10] or in the simulations of its standard mean field continuum description [11].

To get a better understanding of the pattern formation process, we now discuss how to coarse grain the microscopic dynamics (1) to obtain a macroscopic description of the model. On symmetry grounds, there are two candidates for the hydrodynamic fields: the conserved particle density ρ and the local alignment, or polarization, vector **P**. Note that "hydrodynamic" here means slowly varying in space and time—the dynamics of the underlying fluid is not included in our modeling. Following Refs. [20,24], we start with the microscopic Eq. (1) and use Itō calculus to write down a stochastic dynamical equation for the evolution of $f(\mathbf{r}, \theta) = \sum_{j=1}^{N} \delta(\mathbf{r} - r_j)\delta(\theta - \theta_j)$, the microscopic density of particles at position **r** with angle θ, which reads

$$\partial_t f(\mathbf{r}, \theta) + \mathbf{e}_\theta \cdot \nabla[vf]$$
$$= \epsilon \frac{\partial^2 f}{\partial \theta^2} - \frac{\partial}{\partial \theta}\sqrt{2\epsilon f}\,\eta - \gamma \frac{\partial}{\partial \theta} \int d\theta' d\mathbf{r}' f(\mathbf{r}', \theta')$$
$$\times f(\mathbf{r}, \theta)F(\theta' - \theta, \mathbf{r} - \mathbf{r}'). \quad (2)$$

FIG. 1 (color online). (A) Phase diagram in the (ϵ, λ) plane, for $N = 3000$, $L = 10$, $\gamma = 0.16$, $v_0 = 2$, and $v_1 = 0.1$. Blue filled circles on the phase boundary correspond to peaks in the variance of the particle density, while green squares separate states with zero and nonzero mean orientation. Phases are labeled as per discussion in the text. Horizontal and vertical red lines indicate linear instabilities toward clustering and ordering, respectively. (B) Snapshots of the stripy (b), aster (e), moving clumps [d(i)], and lane [d(ii)] patterns. The crosses in A correspond to the snapshots in B. Particles are color coded by direction, with blue (darker gray) horizontal and red (lighter gray) vertical.

The second term on the left-hand side describes familiar advection, but with one important difference: the velocity v appears *inside* the gradient. This is what leads to the instabilities responsible for the new patterns in the simulations. The interaction term in Eq. (2) differs from other models of SP particles where the alignment is explicitly due to "collisions," and the interaction strength depends on v [14,25]. Such cases can be recovered by allowing γ to vary with v. To derive mean-field hydrodynamics equations for the flying XY model, we first drop the noise term, $\sqrt{2\epsilon f}\eta$. Following Bertin, Droz, and Gregoire [25], we Fourier transform Eq. (2) to get equations of motion for $f_k \equiv \int f(\mathbf{r}, \theta)e^{ik\theta}d\theta$. Using $2\pi f(\mathbf{r}, \theta) = \sum_k f_k e^{-ik\theta}$ and $2\pi F(\theta, \mathbf{r}) = \sum_k F_k e^{-ik\theta}$, we obtain a hierarchy of equations:

$$\partial_t f_k + \frac{\partial}{\partial x}\frac{vf_{k+1} + vf_{k-1}}{2} + \frac{\partial}{\partial y}\frac{vf_{k+1} - vf_{k-1}}{2i}$$
$$= -k^2\epsilon f_k + i\frac{\gamma k}{2\pi}\sum_m f_m F_{-m}f_{k-m}, \qquad (3)$$

where all sums run from $-\infty$ to $+\infty$. In principle, F is slightly nonlocal in space so that the second term of the right-hand side of Eq. (3) should retain a spatial integral.

We are, however, interested in the hydrodynamic, large-scale, description of the system, a limit in which R is very small and we assume F to be perfectly local [26]. To obtain mean-field equations for the hydrodynamic variables, we approximate the mesoscopic density of particles $\rho(x, t)$ by the angular average of the microscopic one, i.e., $\rho \equiv f_0$. This can be justified in dense systems [27–29], where interactions are averaged over many neighbors. In a similar fashion, we approximate the x and y component of $\rho\mathbf{P}$ by the real and imaginary part of f_1, respectively. By writing out in full the $k = 0$ case of Eq. (2), we then find that the density field obeys the continuity equation

$$\partial_t\rho = -\nabla \cdot (v\mathbf{W}), \qquad (4)$$

where $\mathbf{W} \equiv \rho\mathbf{P}$. To make further progress, we now assume that we are not too deeply in the ordered phase, so that $f(\theta)$ is to first order approximation homogeneous; hence, higher Fourier components (f_k for $k \geq 3$) may be neglected. Following [25], we further assume that f_2 is a fast variable, so that $\dot{f}_2 \simeq 0$ (this requires $\epsilon \neq 0$). After lengthy but straightforward algebra, we obtain the following equation for $\mathbf{W}$,

$$\partial_t\mathbf{W} + \frac{\gamma}{16\epsilon}(\mathbf{W} \cdot \nabla)(v\mathbf{W}) = \left(\frac{1}{2}\gamma\rho - \epsilon\right)\mathbf{W} - \frac{\gamma^2}{8\epsilon}W^2\mathbf{W} - \frac{1}{2}\nabla(v\rho) + \frac{3\gamma}{16\epsilon}\nabla(vW^2) - \frac{\gamma}{32\epsilon}v\nabla W^2 - \frac{3\gamma}{16\epsilon}\mathbf{W}\nabla \cdot (v\mathbf{W})$$
$$- \frac{\gamma}{8\epsilon}v\mathbf{W}(\nabla \cdot \mathbf{W}) - \frac{\gamma}{8\epsilon}v(\mathbf{W} \cdot \nabla)\mathbf{W} + \mathcal{O}(\nabla^2). \qquad (5)$$

The second term on the left-hand side of Eq. (5) describes self-advection of particles and breaks Galilean invariance [6]. The first two terms on the right-hand side describe the standard spontaneous symmetry breaking leading to polar order and flocking for sufficiently small ϵ in the Vicsek model at $\lambda = 0$. The third, pressurelike term, $-\frac{1}{2}\nabla(v\rho)$, is the most relevant one in our work, as it is responsible for the clustering instability observed in Fig. 1 when $\lambda \neq 0$. Higher order terms in ∇ and $\mathbf{W}$ have minor effects on patterns and will be discussed elsewhere. When v is constant, Eq. (5) reduces to that in Ref. [25], albeit with a different expression for some of the parameters due to differences in the interaction terms defining the microscopic models [25].

Having written down the mean-field equations of motion, Eqs. (4) and (5), we can now assess how their predictions compare with the simulations of the microscopic model. The continuum theory predicts an order-disorder transition at $\epsilon_c = \frac{1}{2}\gamma\rho_0$. For $\epsilon > \epsilon_c$ there is a stable homogeneous disordered state, with $\rho = \rho_0$ and $\mathbf{W} = 0$. For $\epsilon < \epsilon_c$, the equations yield a homogeneous ordered or flocking state with $\rho = \rho_0$ and $\mathbf{W} = W_0\hat{\mathbf{x}}$, where we have chosen the x axis along the direction of broken symmetry and $W_0 = \sqrt{8\epsilon(\epsilon_c - \epsilon)/\gamma^2}$. The mean-field

transition at ϵ_c does not depend on λ and coincides with that of the equilibrium XY model. The order-disorder phase boundary predicted by the theory is compared to its numerical counterpart in Fig. 2(a). We then study the linear stability of the homogeneous disordered state at $\epsilon > \epsilon_c$ against spatially inhomogeneous fluctuations. It is straightforward to show that when $\lambda \neq 0$, the homogeneous disordered phase becomes unstable for all wave numbers when $v(\rho_0) + \rho_0 v'(\rho_0) < 0$. This instability, referred to as a clustering instability, arises due to the term $-\frac{1}{2}\nabla(v\rho)$ in the equation for $\mathbf{W}$. The threshold between
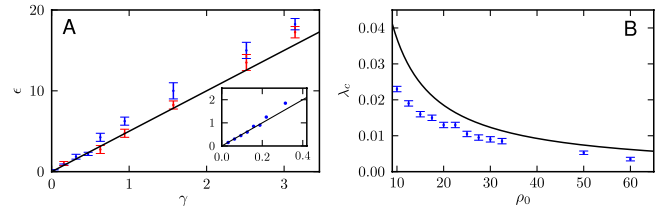

FIG. 2 (color online). (a) Phase boundary for the flying XY model when $\lambda = 0$, showing the critical value of ϵ as a function of γ. Blue (darker gray) points for $v = 2.0$, red (lighter gray) for $v = 0.5$. Inset: data for $v = 2.0$ for smaller values of γ. (b) Phase boundary for $\epsilon = 5$, $\gamma = 0.16$. In all cases $L = 10$ and $N = 1000$.

$\tilde{\lambda}$	0.75	1.5
$\tilde{v}_1$	0.05	0.09
$\tilde{\gamma}$	1.6	3.6
$\tilde{D}$	-	0.02

$\tilde{\lambda}$	1.2	1.5
$\tilde{v}_1$	0.05	0.12
$\tilde{\gamma}$	4.8	4.5
$\tilde{D}$	-	0.02

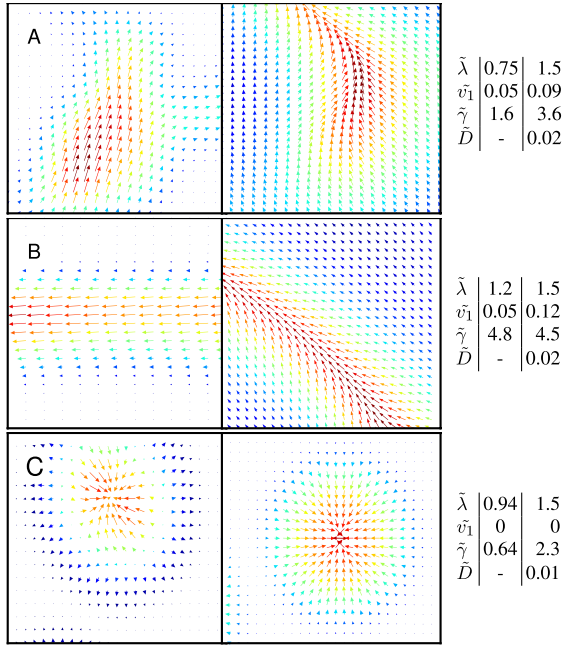|		
$\tilde{\lambda}$	0.94	1.5
$\tilde{v}_1$	0	0
$\tilde{\gamma}$	0.64	2.3
$\tilde{D}$	-	0.01

FIG. 3 (color online). Patterns found for $\lambda \neq 0$ in the microscopic simulations (left column) and in the numerical solution of the hydrodynamic equations (right column). Tables show dimensionless parameter values: $\tilde{\lambda} = \lambda\rho_0$, $\tilde{v}_1 = v_1/v_0$, $\tilde{\gamma} = \gamma\rho_0/\epsilon$, $\tilde{D} = D\epsilon/v_0^2$. Arrows show the **W** field, colors the density [red (gray): high; blue (dark gray): low; yellow (light gray): intermediate]. In the right column, only a fraction of the simulated system is shown for clarity.

homogeneous and clustered phases found numerically at large ϵ is close to but below the prediction [(Fig. 2(b)]. This is reasonable, as the linear stability can only access the spinodal line: fluctuations may trigger phase separation for lower λ.

To go beyond the simple linear stability analysis of the homogeneous disordered state, account for the effect of the nonlinear terms, and, hence, explore the range of patterns compatible with our hydrodynamics equations, we solved Eqs. (4) and (5) numerically, by means of a standard finite difference scheme [23]. In order to enhance the stability of our algorithm, we included a diffusive term $D\nabla^2\rho$ on the right-hand side of Eq. (4). Our numerical results show that all the five patterns, or phases, observed in the microscopic simulations (fluctuating flocking state, moving stripes and lanes, static asters, and moving clumps) can be found within Eqs. (4) and (5)—Fig. 3 portrays a comparison of the $\lambda \neq 0$ patterns. Interestingly, the origin of the atypical asters can be directly read from Eq. (5). In the steady-state, low gradient, small **W** approximation, Eq. (5) reduces to $(\gamma\rho/2 - \epsilon)\mathbf{W} = \nabla(\rho v/2)$ and $\nabla(v\rho)$ thus acts as an ordering field for **W**. Along the radius of an aster, the density increases toward the center, whereas the velocity decreases. Their product can thus be nonmonotonic, which makes **W** change direction, hence the atypical asters seen in the microscopic simulations. In the continuum simula-

tions, even though $\nabla\rho v$ can change sign, the presence of the diffusive terms disallows sharp gradients, and we did not find parameters for which $\nabla\rho v$ was dominating. We could, however, end up with both inward-pointing or outward-pointing asters, corresponding to phases with high-density clumps (at small λ, shown in Fig. 3(c) or low-density voids (at larger λ, similar to those discussed in [5], not shown).

We have shown that a density-dependent motility in our flying XY model, a close relative of the Vicsek model, yields new patterns in suspensions of SP particles. Such patterns include moving clumps, lanes, and asters. All these patterns have experimental counterparts [3–5]. By explicitly linking the microscopic and coarse-grained mean-field dynamics, we were able to identify the key ingredients that trigger the appearance of the new patterns in the "pressure term"— $\frac{1}{2}\nabla(v\rho)$: when this turns negative, new patterns form. Importantly, the patterns we see are not very sensitive to the precise form of $v(\rho)$. For instance, steric hindrance results in velocities that typically decrease linearly with density [29] and would give similar instabilities.

We close with a comparison with other models featuring patterns similar to ours. Continuum equations for microtubule-kinesin solutions leading to aster formation have been proposed in [30]. These included a phenomenological term $\sim S\nabla(\rho)$ with $S > 0$, and ρ the density of motors bound to microtubules, which is similar to our term $-\frac{1}{2}\nabla(v\rho)$. In the $\lambda = 0$ limit, Refs. [11,25] show that asters are absent if the prefactors in the nonlinear terms in the continuum equations are obtained via systematic coarse-graining (however, they do appear if these prefactors are tuned independently [31]).

Finally, Peruani *et al.* [17] studied a microscopic lattice variant of the Vicsek model and also found asters and moving clumps, dubbed traffic jams and gliders. This is again naturally explained by our theory, as their origin in [17] lies in the slowdown of particles due to crowding jamming, which brings up an effective "pressure term" analogous to that in Eq. (5). A density-dependent motility, induced either by steric hindrance or by crosslinkers between actin fibers, may also at the basis of the formation of similar patterns in the actin-walker experiments in [3].

[1] S. Ramaswamy and J. F. Joanny, Nature (London) **467**, 33 (2010); S. Ramaswamy, Annu. Rev. Condens. Matter Phys. **1**, 323 (2010).

[2] D. Bray, *Cell Movements: From Molecules to Motility* (Garland, New York, 2001), 2nd ed.

[3] V. Schaller, C. Weber, C. Semmrich, E. Frey, and A. R. Bausch, Nature (London) **467**, 73 (2010); S. Khler, V. Schaller, and A. R. Bausch, Nature Mater. **10**, 462 (2011);

V. Schaller *et al.*, Proc. Natl. Acad. Sci. U.S.A. (to be published).

[4] J. D. Murray, *Mathematical Biology* (Springer-Verlag, Berlin, 2003), Vol. 2.

[5] R. Thar and M. Kuhl, FEMS Microbiol. Lett. **246,** 75 (2005).

[6] J. Toner and Y. H. Tu, Phys. Rev. Lett. **75,** 4326 (1995); Phys. Rev. E **58,** 4828 (1998); J. Toner, Y. Tu, and S. Ramaswamy, Ann. Phys. (N.Y.) **318,** 170 (2005).

[7] T. Vicsek, A. Czirók, E. Ben-Jacob, I. Cohen, and O. Shochet, Phys. Rev. Lett. **75,** 1226 (1995).

[8] A. Baskaran and M. C. Marchetti, Proc. Natl. Acad. Sci. U.S.A. **106,** 15 567 (2009).

[9] R. A. Simha and S. Ramaswamy, Phys. Rev. Lett. **89,** 058101 (2002).

[10] G. Gregoire and H. Chaté, Phys. Rev. Lett. **92,** 025702 (2004); H. Chaté, F. Ginelli, G. Grégoire, and F. Raynaud, Phys. Rev. E **77,** 046113 (2008).

[11] S. Mishra, A. Baskaran, and M. Cristina Marchetti, Phys. Rev. E **81,** 061916 (2010).

[12] G. Gregoire, H. Chaté, and Y. Tu, Physica (Amsterdam) **181D,** 157 (2003).

[13] F. Peruani, A. Deutsch, and M. Bär, Phys. Rev. E **74,** 030904(R) (2006).

[14] A. Baskaran and M. C. Marchetti, Phys. Rev. Lett. **101,** 268101 (2008).

[15] Y. Yang, V. Marceau, and G. Gompper, Phys. Rev. E **82,** 031904 (2010).

[16] S. Henkes, Y. Fily, and M. Cristina Marchetti, Phys. Rev. E **84,** 040301(R) (2011); S. R. McCandlish, A. Baskaran, and M. F. Hagan, Soft Matter **8,** 2527 (2012).

[17] F. Peruani, T. Klauss, A. Deutsch, and A. Voss-Boehme, Phys. Rev. Lett. **106,** 128101 (2011); F. Ginelli, F. Peruani, M. Bär, and H. Chaté, Phys. Rev. Lett. **104,** 184502 (2010).

[18] One should further distinguish between collection of sterically interacting SP particles where alignment is imposed á la Vicsek and others where it comes solely from steric repulsion of rodlike particles [13–15,17]. In the latter case, steric repulsion yields nematic rather than polar order.

[19] Other functional dependencies lead to a less rich physics—details will be given elsewhere.

[20] J. Tailleur and M. E. Cates, Phys. Rev. Lett. **100,** 218103 (2008); M. E. Cates, D. Marenduzzo, I. Pagonabarraga, and J. Tailleur, Proc. Natl. Acad. Sci. U.S.A. **107,** 11 715 (2010).

[21] C. Liu *et al.*, Science **334,** 238 (2011).

[22] Larger values of N, routinely needed to reliably characterize the nature of the phase transition in Vicsek models [10], lead to negligible corrections for our phase boundary [23].

[23] See Supplemental Material at http://link.aps.org/supplemental/10.1103/PhysRevLett.108.248101 for additional details on finite size effects and on our finite difference simulations of the hydrodynamic equations of motion.

[24] D. S. Dean, J. Phys. A **29,** L613 (1996).

[25] E. Bertin, M. Droz, and G. Gregoire, J. Phys. A **42,** 445001 (2009).

[26] A nonlocal F can be dealt, e.g., as in [20].

[27] H. Zinn-Justin, *Quantum Field Theory and Critical Phenomena* (Clarendon, Oxford, 1989).

[28] J. Tailleur, J. Kurchan, and V. Lecomte, J. Phys. A **41,** 505001 (2008).

[29] A. G. Thompson, J. Tailleur, M. E. Cates, and R. A. Blythe, J. Stat. Mech. (2011) P02029.

[30] H. Y. Lee and M. Kardar, Phys. Rev. E **64,** 056113 (2001); S. Sankararaman and G. I. Menon, Phys. Rev. E **70,** 031905 (2004).

[31] A. Gopinath *et al.*, arXiv:1112.6011 [Phys. Rev. E (to be published)]; K. Gowrishankar and M. Rao, arXiv:1201.3938.